Accurate sound speed estimation for Unmanned Aerial Vehicle-Based Acoustic Atmospheric Tomography

Kevin J. Rogers and Anthony Finn

School of Engineering, the University of South Australia, Australia

ABSTRACT

Acoustic Atmospheric Tomography provides a unique way to measure temperature and wind velocity fields in a slice or volume of atmosphere. There are many applications for these measurements, including atmospheric research, weather forecasting, pollution studies, agricultural monitoring etc. The technique discussed in this paper makes use of an Unmanned Aerial Vehicle that is flown over an array of microphones on the ground. The natural sound emitted by the aircraft is recorded on-board and by the ground microphones. The speed of sound of the intersecting rays are then derived by comparing these measurements. Tomographic inversion is then used to estimate the temperature and wind fields from the sound speed measurements. This technique estimates continuous, three dimensional temperature and wind fields from ground level up to at least 1000 metres. Previous studies have indicated that the sound speed measurements must be accurate to within 0.1% in order to obtain useful results. This paper describes the signal processing techniques that have been employed on field trials data to provide estimates of the atmospheric temperature and wind fields pertaining at that time.

1. INTRODUCTION

Acoustic Atmospheric Tomography (AAT) provides a unique way to measure continuous, distributed 2 or 3-dimensional atmospheric temperature and wind patterns based on sound travel time measurements through an intervening atmosphere. A significant advantage of this technique is that it can generate distributed estimates rather than taking single or multiple point measurements, as is provided by conventional instruments, such a weather balloons, anemometers and SODAR. Comparisons with other techniques and possible applications are described in Ostashev et al. (2008), Rogers and Finn (2013c), Finn and Rogers (2015), Finn and Rogers (2016b). AAT has been under development over the last 30 years. Most experiments have been based on horizontal arrays of mast-mounted speakers and microphones. These primarily take measurements of a horizontal slice near the ground or a low altitude three dimensional volume. Major experiments of this type have been conducted at the University of Leipzig (Arnold et al. 1999, Arnold et al. 2001, Barth et al. 2007, Barth and Raabe 2011) and at the Earth System Research Laboratory (ESRL) in Boulder Colorado (Ostashev et al. 2002, Ostashev et al. 2008). Ostashev et al. (2008) provides an overview of the historical development of AAT.

A technique for performing AAT has been developed where an Unmanned Aerial Vehicle (UAV) is flown over an array of microphones on the ground. The speed of sound between the UAV and the ground microphones is measured and then tomographic techniques are used to calculate the temperature and wind velocity fields (Rogers and Finn 2013c, Rogers and Finn 2013b, Rogers and Finn 2013a, Rogers and Finn 2014). The advantages of this technique are that it can perform AAT of a vertical slice or perform 3-dimensional AAT of a volume above a planar array of microphones up to altitudes in excess of 1 km. This paper describes a technique used to estimate acoustic travel times at levels of accuracy commensurate with 0.1% of sound speed, which have previously been shown to allow faithful tomographic reconstruction (Rogers and Finn 2013c, Finn and Rogers 2015). Travel times are estimated using the natural sound emitted by the UAV.

Figure 1 shows a typical spectrogram for UAV harmonics up to 600 Hz. The UAV used during our field trials has a twin cylinder 4-stroke engine with an exhaust muffler for each cylinder, which is the major source of noise. Harmonics are also generated by the engine and (2-blade) propeller rotation. All of these sound sources are largely synchronous and thus the UAV generates a rich set of acoustic harmonics that are (almost) linearly related and detectable beyond the 30^{th} harmonic. The signal amplitude is larger at low frequencies, but so is the UAV microphone wind noise. The wind noise falls at higher frequencies, which means that the higher harmonics still have reasonable SNRs.

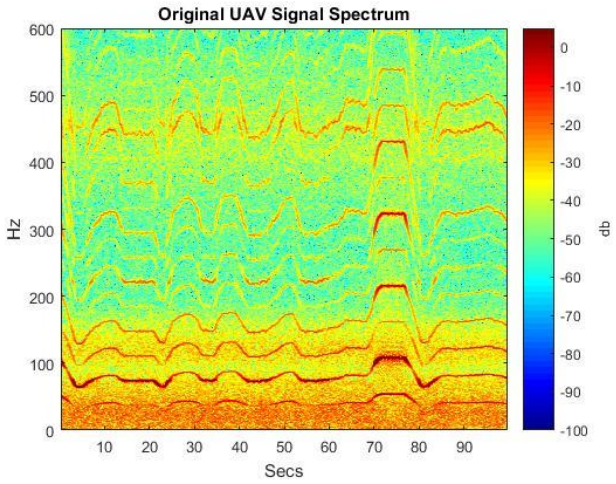

Figure 1: Typical UAV Acoustic Spectrum.

Figure 2 shows a spectrogram of the harmonics that were recorded at a ground microphone for the same period. The received acoustic signal is a time-delayed, frequency-shifted, dispersed and attenuated version of the transmitted signal. The distance between the UAV and the ground microphone varies between 400m and 1300m. As expected, the SNR of each tone is lower than its counterpart in Figure 1, but the UAV harmonics are still largely visible. There are interfering tones and microphone wind noise swamps the first 3 harmonics, despite the use of wind screens. Nevertheless, a significant number of harmonics reach each ground sensor and comparison of the transmitted and received frequencies allows estimation of the travel time by comparing the transmitted and received frequencies. Thus the travel time can be estimated from accurate measurements of frequency at the UAV and the ground microphones.

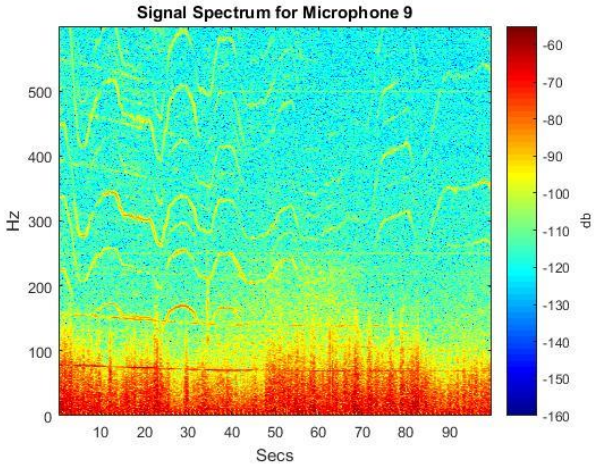

Figure 2: Typical Acoustic Spectrum received by a Ground Microphone

The following section contains the theoretical basis for AAT and travel time estimation. Section 3 describes the field trials and gives the results from the application of the theory to the field trials data. Section 4 provides a discussion and assessment of the results.

2. THEORY

2.1 Acoustic Tomography

AAT exploits the relationship between the speed of sound and the temperature and wind speed. The group velocity of an acoustic ray is affected by temperature and wind speed such that (Ostashev 1997, p.64)

$$\boldsymbol{c} = c_L \boldsymbol{n} + \boldsymbol{v}, \tag{1}$$

where $c_L = \sqrt{\gamma RT}$ is the Laplace speed of sound due to temperature only, $\gamma = 1.4$ is the specific heat ratio, R is the gas constant for air, T is the acoustic virtual temperature ($^\circ K$), $\boldsymbol{n}$ is the normal to the wave front, $\boldsymbol{v}$ is the wind speed vector, and $\boldsymbol{c}$ is the sound speed vector along the ray path. The normal to the phase front can be calculated by firstly calculating the sound speed along the ray path using

$$c = \sqrt{c_L^2 - \boldsymbol{v}\cdot\boldsymbol{v} + (\hat{\boldsymbol{c}}\cdot\boldsymbol{v})^2} + \hat{\boldsymbol{c}}\cdot\boldsymbol{v}, \tag{2}$$

and then from (1)

$$\boldsymbol{n} = \frac{\boldsymbol{c}-\boldsymbol{v}}{c_L}. \tag{3}$$

The travel time along a ray path is

$$\tau = \int_{ray} \frac{1}{|\boldsymbol{c}|} dl \tag{4}$$

where dl is the element of an arc length along the propagation path.

From (1) and (4) the sound wave travel time between a transmitter and receiver is approximately (Ostashev et al. 2008, Wiens and Behrens 2009, Jovanovic 2008)

$$\tau_i = \frac{l_i}{c_0}\left(1 - \frac{\boldsymbol{V_0}\cdot\hat{\boldsymbol{L}}_i}{c_0}\right) - \int_{\boldsymbol{R_{i1}}}^{\boldsymbol{R_{i2}}} \left[\frac{\Delta T(\boldsymbol{R})}{2T_0 c_0} + \frac{\Delta \boldsymbol{V}(\boldsymbol{R})\cdot\hat{\boldsymbol{L}}_i}{c_0^2}\right] dl, \tag{5}$$

where τ_i is the travel time for sound ray i, l_i is the path length for sound ray i, c_0 is the nominal speed of sound, $\boldsymbol{V_0}$ is the mean wind speed vector over the volume, $\widehat{L_i}$ is the unit vector in the direction of sound ray i, $\boldsymbol{R_{i1}}$ is the ray start location (at the UAV), $\boldsymbol{R_{i1}}$ is the ray end location (at a ground microphone), $\Delta T(\boldsymbol{R})$ is the temperature deviation at location $\boldsymbol{R}$ along the ray path, $\Delta \boldsymbol{V}(\boldsymbol{R})$ is the wind velocity deviation at location $\boldsymbol{R}$, and dl is an integration length along the ray's path. The aim of AAT is to estimate the temperature and wind velocity deviations from the travel time measurements.

2.2 Propagation time estimation

Travel times are dependent on the distance between the UAV and the ground microphones and atmospheric conditions and need to be measured with an accuracy of 1 ms or better in order to get wind speed estimates better than +/-1 m/s and temperature estimates within +/- 1 degree C (Finn and Rogers 2015, Finn and Rogers 2016a).

2.2.1 Doppler Method

Initial studies attempted to estimate propagation time from the Doppler Shift. Ostashev (1997, p.160) provides the following equation for the received frequency

$$f_r(t+\tau) = \frac{1+\boldsymbol{n}(t)\cdot\frac{\boldsymbol{v}(t)}{c(t)}}{1+\boldsymbol{n}(t)\cdot\frac{[\boldsymbol{v}(t)-\boldsymbol{u}(t)]}{c(t)}} f_u(t), \tag{6}$$

where $\boldsymbol{n}(t)$ is the unit vector normal to the wavefront at transmit time (t), $\boldsymbol{v}(t)$ is the source wind velocity, $c(t)$ is the Laplace sound speed at the source, $f_u(t)$ is the source frequency (i.e., the UAV harmonic frequencies) and $f_r(t+\tau)$ is the received frequency (i.e., the harmonic frequencies received at each ground microphone) at the receive time. Equation (6) requires that the UAV be equipped with instrumentation to record UAV position, UAV velocity, local wind velocity, local thermodynamic temperature, mixing ratio, specific humidity and relative humidity. Using these measurements, equation (6) can then be used to estimate the travel time by determining the receive time at which

the measured ground frequency best matches the predicted ground frequency (Rogers and Finn 2013b, Finn and Rogers 2016b).

2.2.2 Frequency Integration

An alternative technique is to estimate the travel times by matching the phases of the transmitted and received signals. The travel time corresponds to when the receive phase equals the source phase, i.e.

$$\theta_r(t+\tau) = \theta_u(t). \tag{7}$$

The source and received phases can be calculated by integrating the measured source and received frequencies using

$$\theta_u(t_u) = \theta_u(t_{u0}) + 2\pi \int_{t_{u0}}^{t_u} f_u(t)dt, \text{ and} \tag{8}$$

$$\theta_r(t_r) = \theta_r(t_{r0}) + 2\pi \int_{t_{r0}}^{t_r} f_r(t)dt, \tag{9}$$

where $\theta_u(t_{u0})$ is the phase angle of the transmitted signal at any starting time t_{u0}, $\theta_r(t_{r0})$ is the phase angle of the received signal at any starting time (t_{r0}) and t_r is the receive time. Thus the receive times can be calculated by performing numerical integration of equations (8) and (9), matching the source and receive phases and thus calculating the travel time at any transmit time. However, all of the frequency measurements are subject to measurement errors and so errors in the estimated phases will also accumulate. The net result is that the variance in the estimate of the receive time at measurement i is

$$\sigma_{tr}^2(i) \approx \sigma_{tr}^2(i-1) + \frac{f_{ra}^2(i)\sigma_{f_{ra}}^2(i) + f_{ua}^2(i)\sigma_{f_{ua}}^2(i)}{f_{ra}^4}\Delta t_u^2, \tag{10}$$

where $f_{ra} = f_r(i-1) + f_r(i)$, $f_{ua} = f_u(i-1) + f_u(i)$ and $\Delta t_u = t_u(i) - t_u(i-1)$. The receive time estimates will accumulate errors. Thus the net effect is that the frequency integration technique is very good at tracking short term transients but is subject to long term drift and needs to be supplemented by another technique to provide an initial estimate of starting conditions and to correct for the long term drift. The Doppler Method provides an absolute estimate of frequency that can potentially be used to obtain an absolute measure of the speed of sound. However, this tends to be sensitive to noise. An alternative technique is to calculate the speed of sound at the source and receiver from local environmental measurements and then use the mean of these values to estimate the average value over the ray path. The sound speed estimate is not exact, but a standard deviation can be applied to it. Thus, the independent estimate of the arrival time is

$$t_{rav}(i) = t_u(i) + l(i)/c_{av}(i), \tag{11}$$

where $l(i)$ is the distance between the source and the receiver at the transmit time, c_{av} is the average of the sound speed at the source and receiver, and t_{rav} is the calculated arrival time based on the average sound speed. The range is known with a high level of accuracy and so most of the variance is due to uncertainty in the average sound speed. Thus

$$\sigma_{t_{rav}}^2(i) = \frac{l^2(i)}{c_{av}^4(i)}\sigma_{c_{av}}^2(i). \tag{12}$$

The frequency integration and average estimates can then be combined to provide a composite estimate of the receive time, such that

$$t_{rc}(i) = \frac{I_{av}(i)t_{rav} + I_{int}(i)t_r(i)}{I_t(i)}, \text{ and} \tag{13}$$

$$\sigma_{rc}^2(i) = \frac{1}{I_t(i)}, \quad (14)$$

where $t_{rc}(i)$ is the composite estimate of the receive time at epoch i, $\sigma_{rc}^2(i)$ is the variance of the composite arrival time, $I_{av}(i) = 1/\sigma_{t_{rav}}^2(i)$ is the Fisher information for the average receive time estimate, $I_{int}(i) = 1/\sigma_{t_r}^2(i)$ is the Fisher information for the frequency integration receive time estimate and $I_t(i) = I_{av}(i) + I_{int}(i)$ is the total Fisher information for the composite receive time estimate. Equations (13) and (14) are executed successively for each epoch. The average time estimate synchronizes the initial phases for the transmitter and receiver and compensates for drift. The frequency integration estimate provides deviations from the average and substantially overcomes any bias that may be present in the average estimate.

2.3 Frequency Measurement

The travel time estimates are highly reliant on accurate frequency measurements at the UAV and the ground microphones. The UAV is equipped with an encoder that provides estimates of the engine rotation rate. The RPM readings are provided at a rate of approximately 1 Hz, which gives an approximate indication of UAV emitted frequencies, but it is not exact and there is also some latency. However, it is useful as an initial estimate of the expected frequency and the harmonic structure.

2.3.1 Resampling

When the frequency changes rapidly with respect to time (e.g., due to autopilot control variation), the frequency measured by the Fast Fourier Transform (FFT) gets "smeared", the SNR is reduced and it is difficult to get an accurate estimate of instantaneous frequency. In addition, if the frequency acceleration varies during a sampling window, then the average frequency estimate will be biased due to the curvature in instantaneous frequency versus time. In order to overcome this smearing and bias the signal is resampled in the time domain (based on the expected frequency) to normalize the expected frequency spectrum. For the UAV, the expected frequency is derived from the UAV's engine rotation rate. The expected frequency at each ground microphone is estimated using the measured UAV frequency and the Doppler equation for nominal wind and temperature conditions. If the original continuous signal, $x(t)$, is digitized at a constant sampling rate of F_s samples/second, then the i_{th} signal sample is $x_i = x\left(\frac{i}{F_s}\right)$. If the expected frequency is $f(t)$, then the expected signal phase is

$$\theta(t) = 2\pi \int_{t_0}^{t} f(\lambda) d\lambda. \quad (15)$$

The phase relationship can be inverted to express time as a function of phase such that $t = t(\theta)$. If the signal is resampled at constant phase steps (by interpolating x_i), then the i_{th} value of the resampled signal is $y_i = x(t(i\Delta\theta))$. If there are n samples, then the k_{th} component of the N point Discrete Fourier Transform (DFT) of y_i will be

$$Y_k = \sum_{i=0}^{n-1} y_i e^{-\frac{j2\pi ik}{N}} \quad (16)$$

and the resampled spectrum will have a constant expected frequency of $f_0 = \frac{2\pi F_s}{\Delta\theta N}$.

Figure 3 illustrates the effect of resampling the UAV acoustic signal. The resulting harmonic frequencies are nearly constant with respect to time. Slight variations in the frequency tones are due to inaccuracies in the expected frequency. However, the resampled signal provides a good basis for frequency measurements, which enables longer frequency sampling times, the elimination of smearing and bias, higher SNR and improved frequency estimates. Once the frequencies have been estimated in the resampled domain, then the resampling process can be inverted to produce frequency estimates in the original time domain.

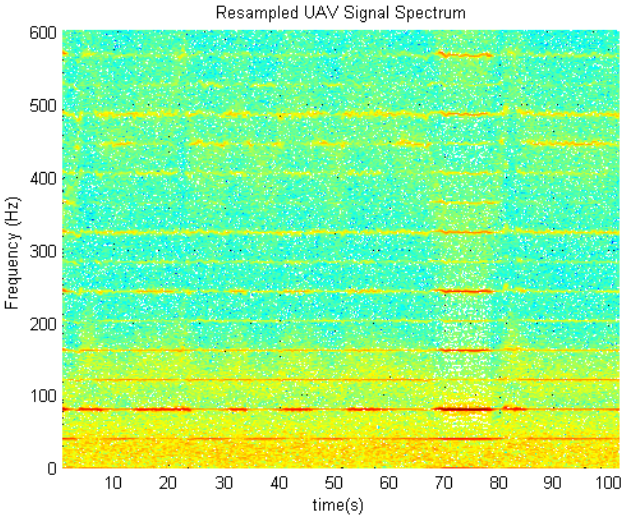

Figure 3: Resampled UAV Signal Spectrum

2.3.2 Measuring harmonic frequencies

Once the signal has been resampled, the expected frequency is known approximately and the amplitude, frequency and local noise power may be estimated for each harmonic. Frequency measurements are used for travel time estimation and the amplitude and noise variance are used to weight the observations in the tomographic inversion.

During each sampling window, each resampled harmonic is considered to be a constant frequency sinusoid of the form

$$x(t) = a_0 \cos(2\pi f_0 t + \theta_0) \tag{17}$$

for $-\frac{T}{2} \leq t \leq \frac{T}{2}$, where a_0 is the sinusoid amplitude, f_0 is the frequency, θ_0 is the phase and T is the duration (1 second) of each resampled window. However, the pure signal is corrupted by noise such that the observed signal is

$$y(t) = x(t) + \gamma(t), \tag{18}$$

where $\gamma(t)$ is measurement error, which is assumed to be Gaussian white noise.

There are many methods available for frequency estimation. The chosen method was to perform a least squares fit for the residuals for the DFT of the recorded signals. Thus the aim is to select a_0, f_0, and θ_0 to minimize

$$E = \sum_{k=k_1}^{k_2} |X_k - Y_k|^2, \tag{19}$$

where X_k is the DFT of x and Y_k is the DFT of y. Minimization is performed using the Newton Raphson method and the noise variance is estimated from the residuals.

Simulation studies have indicated that this technique performs near the Cramer Rao Lower Bound (CRLB) as given by Castanié (2013, pp.72-73). In practice the SNR is relatively low for many harmonics (especially at the ground sensors) and it is common for a noise peak to be greater than the true signal, which can result in the frequency estimator locking onto a false value. However, since all of the harmonics are derived from the same shaft speed, the harmonics should all be closely linearly related, which is exploited to reject frequency estimates that are inconsistent

with others. Once a valid set of harmonic estimates is resolved, then the fundamental is estimated using weighted least squares and a composite variance is calculated for the fundamental, based on the SNRs and the CRLB estimates (Rogers and Finn 2013b).

3. RESULTS FROM FIELD TRIALS

3.1 Field trials equipment

Field trials were conducted at an airfield at Saint Leonards, Victoria on the 10th and 11th of June, 2015, which was an overcast winter's day with light winds. An Aerosonde MK 4.7 UAV was flown over an array of microphones on the ground. The UAV was propelled by a twin cylinder 4-stroke engine with 2 exhaust mufflers, one for each cylinder. The exhausts are the major source of noise, although significant noise is also emitted from the rotation of the engine crankshaft, the rear mounted two blade propeller, distributed aircraft vibration and aerodynamic noise. Each exhaust emits an exhaust pulse alternately for every second rotation of the engine. The UAV's acoustic emissions were sampled at 51.2 kHz synchronously with the 1 pulse per second reference of the GPS onboard the UAV. The UAV was fitted with a Real Time Kinematic (RTK) Carrier Phase (CP) Differential Global Positioning System (DGPS), which enabled position recording with an accuracy better than 3 cm at 20 Hz. The UAV recorded GPS velocity, horizontal wind speed and direction, air temperature, mixing ratio, specific humidity, engine rotation rate in revolutions per minute (rpm), and the signature of the UAV's acoustic emissions.

The ground array comprised a line of 28 ECM800 10mV/Pa condenser microphones sampled at 44.1kHz using four 8-channel 24 bit Data Acquisition (DAQ) recorders. Each recorder recorded 7 microphones and the remaining channel recorded a GPS derived 1 Pulse Per Second (PPS) signal to provide an absolute timing reference for the microphone signals. Additional meteorological equipment was also used for validating or supplementing the AAT test results, which included a Fulcrum3D Sonic Detection and Ranging (SODAR) station, two Windmaster Ultrasonic Anemometers, 4 Hobo Pro v2 loggers (for temperature and humidity recordings) and a Digitech Professional Weather Station. These were distributed along the microphone array and their positions were accurately recorded using an RTK CP DGPS.

3.2 Flight scenario

The microphones were located in a line adjacent to the main runway. The UAV flew directly above the microphones at heights between 300 and 500 metres. The scenario was completed in just under 720 seconds, but each overflight lasted only 20 seconds. The tomographic region is the region where the temperature and wind fields are estimated, which is a 500 metre vertical slice above the line of ground microphones.

3.3 Frequency measurement results

The fundamental frequencies are generally in the range from 35 to 55 Hz. Based on the CRLB, the measured SNRs indicate that the frequency measurement accuracy should be typically 1.3 milliHertz for the UAV and about 2.5 milliHertz on the ground. However, in practice, these accuracies are not currently achieved because the harmonics are only approximately multiples of the fundamental, e.g., because of variation in the timing and acoustic characteristics of engine combustion. The fundamental frequency has been estimated by dividing each harmonic frequency by the harmonic number and then averaging them. The normalized harmonics typically have a standard deviation of approximately 35 milliHertz, which means that our ability to measure each harmonic frequency accurately is not critical, as the errors will be swamped by the non-linearity in the harmonic relationships. Despite this, the net result still represents an error of approximately 0.1% for each fundamental frequency measurement, which has previously been shown to represent the threshold for which faithful tomographic reconstructions can be achieved.

3.4 Doppler Results

Various tests were performed to estimate ray travel times using the Doppler technique. The Doppler technique requires the ground frequency to be changing rapidly in order to get a reasonable estimate of τ (Finn and Rogers 2016b), which occurs when the UAV passes over the top of a microphone or if the UAV frequency is changing rapidly due to autopilot control requirements. The Doppler technique is thus extremely sensitive to frequency measurement errors, especially during periods when the received frequency changes only slowly with respect to time. Figure 4 shows estimates of sound ray speeds from the field trial recordings for a single microphone. The estimates are

clustered around 339 m/s. There is also a slightly rising trend, as expected, as the UAV was progressively descending during this scenario and the average sound speed therefore increases. However, the estimate errors are quite large.

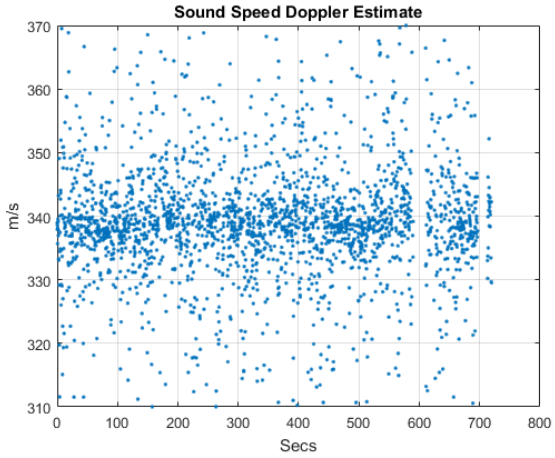

Figure 4: Sound speed estimates using the Doppler Method for a single microphone.

3.5 Frequency integration results

Figure 5 shows the results from using the frequency integration method for estimating ray sound speed for all 26 microphones over a 720 second scenario. All microphones yield similar results for the speed of sound even though they are independently estimated. There are a few outliers. These occur mainly when the received SNR is low, which is usually when the UAV is outside the tomographic region. The speed of sound varies over a small range between 337 and 339 m/s, which is expected, as the trials were conducted on a cool overcast day with very little wind. These results illustrate that the frequency integration technique is significantly better than the Doppler technique.

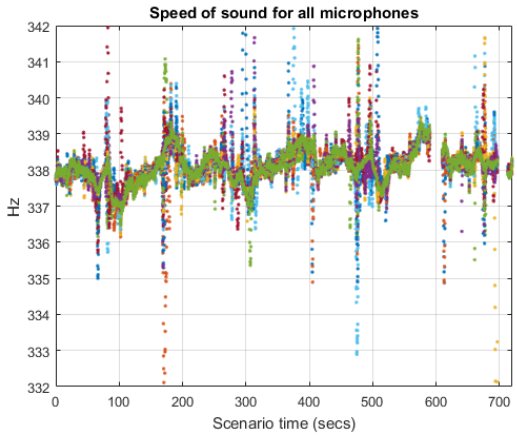

Figure 5: Sound Speed Estimates using the Integration technique for all 26 microphones.

3.6 Tomographic reconstruction

The tomographic inversions are performed by modelling the temperature and wind fields as the sum of a uniform lattice of 7 horizontal by 5 vertical weighted Radial Basis Functions (RBFs) and the RBF weights estimated using a Tikhonov regularised least squares adjustment, as per (Finn and Rogers 2015). The RBF centres were located within the limits described by the flight path of the UAV and microphone array. Figure 6 shows wind contours in the x-z plane plotted over the temperature profile, the x-axis representing the baseline along the array of 28 microphones (with positive x oriented roughly due west). The tomographic estimates of wind speed closely align with independent SODAR estimates.

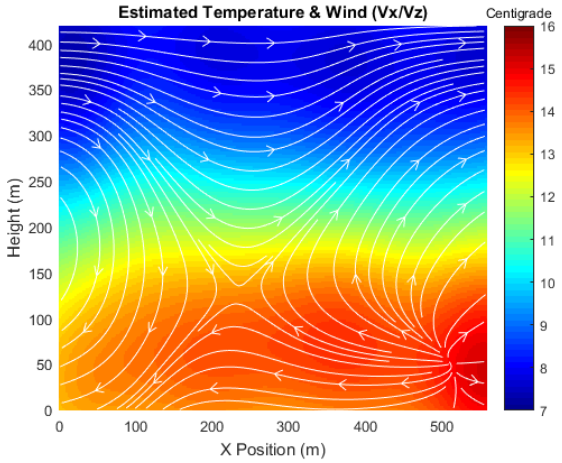

Figure 6: Tomographic estimates of wind contours and temperature in the x-z plane

4. DISCUSSION

The use of the UAV as a sound source has advantages and disadvantages. The spectrum of the sound source is not well controlled, as the frequency is constantly changing due to the action of the UAV's autopilot. The sound power is also distributed over multiple narrowband harmonic tones and each harmonic has a low Signal to Noise Ratio (SNR) that often disappears below the noise floor. A synthesized signal is better defined and is easier to process, but a high powered signal source requires significant additional payload, space and power. The frequencies of individual harmonics can be measured with a high level of accuracy, but the harmonics are not exactly linearly related, which means that the composite fundamental frequency is not absolutely well-defined, which is the major cause of variance in measuring instantaneous frequency both at the UAV and on the ground. Thus, the measurement accuracy for individual harmonics is not critical, as accuracy is dominated by the non-linear harmonic relationships. Nevertheless, the speed of each sound ray can be estimated with an accuracy of the order of 0.1% by using the frequency integration method. The Doppler method requires rapid changes in the received frequency whereas this is not necessary for the frequency integration method.

5. CONCLUSION

This paper presents a technique for determining sound speed between a UAV and an array of ground receivers by integrating the received frequency of the natural acoustic signature of the UAV. The estimates of sound speed derived using the frequency integration method applied to the natural sound emitted by the UAV have achieved the levels of accuracy that are needed for faithful reconstruction of atmospheric temperature and wind profiles. Thus UAV based acoustic atmospheric tomography has potential for accurately estimating continuous temperature and wind fields in the lower regions of the Atmospheric Surface Layer.

ACKNOWLEDGEMENTS

The authors are grateful to both the Australian Research Council and the Sir Ross and Sir Keith Smith Fund for their support for this project. We are also grateful to Maurice Gonella of Aerosonde, Peter May and John Nairn of the Bureau of Meteorology (BoM), and Greg Holland and James Done of the National Center for Atmospheric Research (NCAR). Their ongoing assistance and support in this project is most valuable.

REFERENCES

Arnold, K., Ziemann, A. & Raabe, A. 1999. *Acoustic tomography inside the atmospheric boundary layer*. Physics and Chemistry of the Earth, Part B: Hydrology, Oceans and Atmosphere, 24, 133-137.

Arnold, K., Ziemann, A. & Raabe, A. 2001. *Tomographic monitoring of wind and temperature at different heights above the ground*. Computers, IEEE Transactions on, 87, 703-708.

Barth, M. & Raabe, A. 2011. *Acoustic tomographic imaging of temperature and flow fields in air*. Measurement Science and Technology*,* 22**,** 035102.

Barth, M., Raabe, A., Arnold, K., Resagk, C. & Du Puits, R. 2007. *Flow field detection using acoustic travel time tomography*. Meteorologische Zeitschrift*,* 16**,** 443-450.

Castanié, F. 2013. *Digital spectral analysis: parametric, non-parametric and advanced methods*, John Wiley & Sons.

Finn, A. & Rogers, K. 2015. *The feasibility of unmanned aerial vehicle-based acoustic atmospheric tomography*. The Journal of the Acoustical Society of America*,* 138**,** 874-889.

Finn, A. & Rogers, K. 2016a. *Accuracy requirements for unmanned aerial vehicle-based acoustic atmospheric tomography*. The Journal of the Acoustical Society of America*,* 139**,** 2097-2097.

Finn, A. & Rogers, K. 2016b. *Improving Unmanned Aerial Vehicle-Based Acoustic Atmospheric Tomography by Varying the Engine Firing Rate of the Aircraft*. Journal of Atmospheric and Oceanic Technology.

Jovanovic, I. 2008. *Inverse Problems in Acoustic Tomography: Theory and Applications.* PhD thesis, EPFL, Lausanne, Switzerland.

Ostashev, V. 1997. *Acoustics in moving inhomogeneous media*, CRC Press.

Ostashev, V., Bedard, A. & Voronovich, A. *Array for acoustic tomography of the atmosphere*. Geoscience and Remote Sensing Symposium, 2002. IGARSS'02. 2002 IEEE International, 2002. IEEE, 862-864.

Ostashev, V., Vecherin, S. N., Wilson, D. K., Ziemann, A. & Goedecke, G. H. *Recent progress in acoustic tomography of the atmosphere*. IOP Conference Series: Earth and Environmental Science, 2008. IOP Publishing, 012008.

Rogers, K. J. & Finn, A. 2013a. *3D UAV-based atmospheric tomography: Preliminary trials results*. Proceedings of the Australian Acoustical Society Conference, Victor Harbour.

Rogers, K. J. & Finn, A. *Frequency estimation for 3d atmospheric tomography using unmanned aerial vehicles*. Intelligent Sensors, Sensor Networks and Information Processing, 2013 IEEE Eighth International Conference on, 2013b. IEEE, 390-395.

Rogers, K. J. & Finn, A. 2013c. *Three-Dimensional UAV-Based Atmospheric Tomography*. Journal of Atmospheric and Oceanic Technology*,* 30**,** 336-344.

Rogers, K. J. & Finn, A. *3D acoustic atmospheric tomography*. SPIE Remote Sensing, 2014. International Society for Optics and Photonics, 92420R-92420R-9.

Wiens, T. & Behrens, P. 2009. *Turbulent flow sensing using acoustic tomography*. Proc. Inter-Noise 2009: Innovations in Practical Noise Control.